

Gold nanorods mediated controlled release of doxorubicin: nano-needles for efficient drug delivery

Sunil Pandey · Ritu Shah · Ashmi Mewada ·
Mukeshchand Thakur · Goldie Oza ·
Madhuri Sharon

Received: 6 September 2012 / Accepted: 10 March 2013 / Published online: 23 March 2013
© Springer Science+Business Media New York 2013

Abstract Use of cysteamine hydrochloride (Cys-HCl) protected gold nanorods (GNRs) as efficient carrier of widely used anti-cancer drug doxorubicin using folic acid as navigational molecule is presented in this work. GNRs were found to have excellent drug loading capacity of >97 %. A detailed comprehension of in vitro drug release profile under ideal physiological condition was found to obey 1st order kinetics at pH 6.8, 5.3 and 7.2, an ideal milieu for drug delivery to solid tumours.

1 Introduction

Nano-particulate drug delivery systems containing anti-cancer agents have received much attention due to their unique accumulation behaviour at the tumor site [1–3]. Enhanced permeation and retention effect is now considered as a major mechanism for their unique biodistribution profile in the tumour tissue [4, 5]. The environmental acidity significantly influences response of cancer cells to various treatments [6–10]. The intracellular and extracellular pH gradient in tumor cells is maintained by complicated biophysical mechanisms [6, 7, 11]. Various targeting moieties or ligands against tumor-cell-specific receptors have been immobilized on the surface of nano-particulate

carriers to deliver them within cells via receptor-mediated endocytosis. Among them, vitamin M also known as folic acid (FA) or folate has been widely employed as a targeting moiety for various anti-cancer drugs [12–16]. Folate binding protein, a glycosyl phosphatidyl inositol (GPI) anchored cell surface receptor for folate, has been known to be over expressed in several human tumors including ovarian and breast cancers, while it is highly restricted in normal tissues [17]. For this reason, FA has been covalently conjugated to anti-cancer drugs and liposomes for the purpose of selective targeting against tumors [15, 16]. A folate group covalently attached to phospholipids or cholesterol was used to form doxorubicin (DOX) encapsulated liposomes. These liposomes conjugated with FA showed selective targeting effect on human carcinoma with reducing cardiac toxicity of DOX [17]. An attempt has been made by the authors to comprehend the different variable parameters involved in GNRs synthesis and impact of each parameter on the overall reaction during the formation of GNRs [18]. The authors have also optimized fabrication of GNR of desired aspect ratios [19].

Exploiting metal nanoparticles for ferrying drug to the target is a key technology for the realization of nano-medicine. It has potential to enhance drug bioavailability and improve the timed release of drug molecules, and enable precision drug targeting [20–22]. Nano scale drug delivery systems can be implemented within pulmonary therapies [23], as gene delivery vectors [24], and in stabilization of drug molecules that would otherwise degrade too rapidly [25, 26]. GNRs with suitable aspect ratios can absorb and scatter strongly in the NIR region, which can be used for enhanced optical imaging and photo-thermal cancer therapy. Due to its tunable optical properties (dependent upon the aspect ratio) and chemical versatility, GNRs have been explored for a broad spectrum of biomedical applications

Sunil Pandey and Ritu Shah contributed equally to this study.

S. Pandey (✉) · R. Shah · A. Mewada · M. Thakur · G. Oza ·
M. Sharon
N. S. N. Research Centre for Nanotechnology and
Bionanotechnology, Jambhul Phata, Ambernath (W) 421 505,
Maharashtra, India
e-mail: gurus.spandey@gmail.com

M. Sharon
e-mail: sharonmadhuri@gmail.com

including drug/gene delivery and photo-thermal therapy, as well as computed tomography and/or optical imaging [27]. Reports on Functionalization of GNRs are available where stabilization of GNR was successfully done using Polyethylene glycol (PEG). A detailed study on drug release using GNRs was reported previously using PEG modified DOX [27]. Additional benefits of using targeted nanoscale drug carriers are reduced drug toxicity and more efficient drug distribution [28].

An ideal kinetic profile of drug release from a prolonged release carrier is a zero order curve. The constant amount of an active substance dosed within time unit provides the drug presence at a therapeutic level in human body during the long time period. In the literature, plenty of theoretical or empirical release models are described [29–31]. Korsmeyer–Peppas, first order kinetics and Gallagher and Corrigan [32] models have been chosen to describe the ibuprofen (IBU) release from polylactide microspheres incorporated in chitosan films.

In this experimental work, seed mediated method was used to fabricate GNRs of moderate aspect ratio for synaptic delivery DOX is presented. FA, due to its abundance at the surface of cancer cells, were used as molecular compass for specific interactions of the drug-GNR conjugate with cancer cells. In a recent study [33], it was deciphered that rod shaped nanoparticles are much superior in ferrying therapeutic payloads to cancer cells due to their favourable cross-talks with immune cells.

Additionally, a detailed investigation of the drug-GNR confrontation in terms of loading and release of the drug under physiological as well as tumorous milieu (pH 5.3, 6.8 and 7.2) is done using ideal statistical models.

2 Materials and methods

For drug delivery studies GNRs were synthesized using seed mediated method [19] with an aspect ratio of 4–5. To synthesize seed solution, 2.5 ml of 1 mM of HAuCl_4 was added to 5 ml of 0.2 M cetyl trimethyl ammonium bromide (CTAB) (Sigma Aldrich, USA). To this solution, 600 μl of pre-chilled 10 mM sodium borohydride (Merk, Germany) was added under vigorous stirring condition forming pale yellow coloured solution. The experiment was performed at 20 °C using Nanopure water (18 M Ω). Growth solution for GNRs was prepared by 2.5 ml of 1 mM HAuCl_4 (Sigma Aldrich, USA) in 2.5 ml of 0.2 M CTAB. 113 μl of 4 mM AgNO_3 (Alfa Aesar, USA) and 35 μl of 78.8 mM ascorbic acid (Merk, Germany) were added to this solution followed by gentle agitation forming a transparent growth solution. 4 μl of seed solution was transferred into unstirred growth solution and the reaction was allowed to take place for 2 h till the solution turns reddish blue.

The spectrophotometric analysis of the colloidal solutions was carried out using UV–Vis spectrophotometer (Lambda 25, Perkin Elmer). Morphological details of the synthesized GNR were studied using transmission electron microscope (TEM) (Zeiss Microimaging GmbH, Germany) and field emission gun-scanning electron microscope (FEG-SEM) (Zeiss Microimaging GmbH, Germany). The samples were purified by centrifuging at 5,000 rpm and then the pellet deposited at the side walls as well as bottom of the test tube was separated and loaded on to formvar coated copper grid and silicon substrate for TEM and FEG-SEM analysis. Fourier transform infra-red (FTIR) spectroscopy (Bruker) studies were performed within the spectral window 500–4,000 cm^{-1} . For Inductively coupled plasma atomic emission spectroscopy (ICPAES) (ARCOS Spectro, Germany), GNR solution was diluted with ultra-pure D/W and injected into the nozzle at high temperature.

2.1 Functionalization of GNR using Cys-HCl

GNRs were functionalized using Cys-HCl as a linker. The attachment of Cys-HCl linker was done by considering ratios of GNR:Cys-HCl as 1:130 and 1:200. The solutions were kept undisturbed for 2 h at 28 ± 2 °C. The linker attachment was verified by visual inspection in the form of color change as well as using UV–Vis spectroscopy. Deeper intricacies of the drug–GNR interaction were studied using FTIR.

2.2 Activation and attachment of FA to GNR–Cys conjugate

FA was activated by dissolving 0.25 g of FA into 20 ml of DMSO (dimethylsulfoxide) and the mixture was subjected to sonication for 45 min. The carboxylate group of FA was activated by addition of 0.225 gm of NHS (*n*-hydroxy-succinimide) and 0.125 gm of DCC (dicarboxy aminocarbodiimide). The reaction was allowed to take place in inert environment created by nitrogen gas at 28 ± 2 °C for 12 h (FA/NHS/DCC molar ratio 2:2:1). The resultant mixture was filtered through Whatman filter paper and was used for further characterization. Attachment of FA is facilitated by adding 9 ml of GNR with Cys-HCl linker (1:160) and 1 ml of activated FA. The color of the solution became pale violet. The solution was later subjected to purging under N_2 atmosphere for 4 h and stirred continuously using a magnetic stirrer. After 4 h, both inlet and outlet valves were closed. The reaction was allowed to take place for 24 h. After completing the reaction for 24 h, the mixture was filtered using Whatman paper and stored at 20 °C. Free FA was removed using 3,000 kDa Dialysis bag against Phosphate buffer saline (PBS), pH 7.2. The post-dialysed samples were centrifuged at 6,000 rpm for 15 min at

20 °C. The pellet was re-dialysed against deionized water for 24 h under continuous stirring. The samples were subjected to UV–Vis spectroscopy at regular intervals to study the attachment.

2.3 Attachment of DOX

10 ml of DOX (0.125 mM) was added to GNR–FA complex along with TEA (triethylamine). The volume was adjusted to 25–30 ml using DMSO. The solution was purged using argon till the color of the solution becomes orange. Purging was continued for 4 h under stirring. After 4 h, both inlet and outlet valves were closed. This setup was stirred continuously for 24 h. UV–Vis spectroscopy was performed at regular intervals. The resultant GNR–CYS–FA–DOX conjugate was purified using extensive dialysis against nanopure water for 3 days using a dialysis tubing (MW cut-off of 3,000 Da to remove the excess amount of unbound DOX molecules and DMSO. The water was exchanged at 6 h intervals. The whole complex was characterized using UV–Vis spectrophotometer and FTIR.

2.4 Drug loading efficiency (DLE)

From the total concentration of DOX used for attachment onto folate conjugated GNR, some of it remains unattached. Hence, it becomes necessary to carry out an experiment for understanding the exact amount of drug that has actually got attached to GNR. 5–6 ml of drug attached complex was centrifuged at 6,000 rpm for 15 min at 20 °C and dialyzed against water to remove the unbound drug. Concentration of DOX was calculated using UV–Vis spectroscopy at 485 nm. Drug loading efficiency (DLE) was calculated using the formula given below.

$$\text{DLE} = \frac{\text{Theoretical amount of drug loaded} - \text{Free drug}}{\text{Theoretical amount of drug loaded}} \times 100 \quad (1)$$

2.5 In vitro release of DOX

GNR–CYS–FA–DOX conjugate was placed in three different dialysis bags (MW cutoff 12–14 kDa, pore size 2.4 nm) to comprehend drug release at pH 5.3, 6.8 and 7.2 using PBS. Former pH values (5.3 and 6.8) correspond to cancerous cells of different origin and physiology. Each sample was initially dialysed against nanopure water in order to remove unbound moieties. After this step, samples were dialysed using PBS at above mentioned pH values. In order to find out the concentration of DOX with respect to time, 3 ml of the buffer medium was taken out at an

interval of 30 min and its absorbance at 485 nm was recorded. This experiment was repeated three times in order use the values for finding out kinetic profile of drug release under physiological conditions.

2.6 Drug release kinetics

A Precise control of the drug carrier architecture, the release of the drug can be tuned to achieve a desired kinetic profile. Three of the most common kinetic profiles are zero order, first order, Higuchi and Hixson–Crowel; these are depicted below and expressed mathematically in Eqs. (2)–(5).

$$\text{Zero order: } Q_0 = Q_0 + K_0 t \quad (2)$$

$$\text{First order: } \ln Q_t = \ln Q_0 + k_1 t \quad (3)$$

$$\text{Higuchi: } Q_t = Q_0 = k_H t^{1/2} \quad (4)$$

$$\text{Hixson crowel: } \sqrt[3]{Q_0} - \sqrt[3]{Q_t} = k_{H,C} t \quad (5)$$

where Q_t is the amount of drug released at time t , Q_0 is the initial amount of drug loaded, k_0 is the zero order release constant, k_1 is the first order release constant, and k_H is the Higuchi release constant.

3 Results and discussion

Synthesis of the GNRs using seed mediated method lead to formation of stable and monodisperse GNRs with an aspect ratio 4–5 [19]. Appearance of purple colour signifies the formation of GNRs with longitudinal and transverse peaks at 527 and 809 nm respectively (Fig. 1a). Purple color becomes more intense when the De-Broglie wavelength of the valence electrons becomes equal to or less than the size of the particle [34]. Due to this phenomenon, freely mobile electrons are caged in GNRs and exhibit a characteristic collective coherent oscillation of plasmon resonance giving rise to surface plasmon resonance (SPR). The plasmon absorption splits into two bands corresponding to the oscillation of the free electrons along and perpendicular to the long axis of the rods [35, 36]. The transverse mode (transverse surface plasmon peak: TSP) shows a resonance at around 520 nm, while the resonance of the longitudinal mode (longitudinal surface plasmon peak: LSP) occurs at higher wavelength and strongly depends on the aspect ratio of nanorods. As aspect ratio is increased, the longitudinal peak is red shifted. To account for the optical properties of GNRs, it has been common to treat them as ellipsoids, which allows the Gans formula (extension of Mie theory) to be applied [35, 37]. Also, the selective area electron dispersion pattern in Fig. 1c depicts that GNRs formed is

crystalline in nature. Figure 1c, d shows TEM image of purified GNRs synthesised using seed mediated method.

3.1 Detection of gold using ICPAES

Conversion of Au^{3+} from HAuCl_4 into the growth solution of GNRs was calculated using inductive coupled plasma atomic emission spectroscopy (ICPAES). The conversion rate of gold was calculated to be 17 %, with a concentration of 0.17 mM (35.064 ppm) which was present in the growth solution of GNRs against the original concentration of gold which was 1 mM.

3.2 Surface functionalization of GNRs using Cys-HCl

The surface affinity of the GNRs towards thiols and amines can be exploited to attach Cys-HCl in various ratios. The studies revealed that the ratio 1:160 (GNR:Cys-HCl) was more promising.

There was significant red shift (from 837 to 845 nm) in LSPR peak as seen in Fig. 2. The red shift is observed due to the chemical reaction between the surface of the GNR i.e. CTA^+ and the linker [38–41]. This can also be credited to change in the refractive indices of both, the solution as well as GNRs. Moreover, another reason may be that Cys-HCl has

a strong affinity towards Au due to the presence of thiol groups ($-\text{SH}$). The inherent reactivity of gold nanorod is due to caging of its electrons in a box of infinite work function. This inspires these electrons to react with tremendous efficiency to form stable bonds.

Figure 3 illustrates a comparative study of FTIR spectra of purified GNRs, thiol based linker Cys-HCl and GNR–Cys-HCl conjugate. Appearance of peaks at 2,853 and 2,921 cm^{-1} in Fig. 3a corresponds to SH stretch. The bond must have formed due to asymmetric interaction between CTA^+ of GNRs and thiol ($-\text{SH}$) of cysteamine hydrochloride. Thiol bond has a higher affinity towards gold followed by amine group [38–41]. Here the interaction between SH and GNR is prominent as the pH of the colloidal solution of GNR is acidic [18, 19, 35]. Hence, the amine end of the linker i.e. Cys-HCl remains free for FA attachment.

The schematic representation of the reaction between GNR and Cys-HCl (Fig. 4) can be proposed as:

3.3 Orchestration of GNR–cysteamine conjugate by activated FA

Orchestration of GNR–Cys-HCl conjugate with activated folic acid was authenticated by their relative FTIR spectra

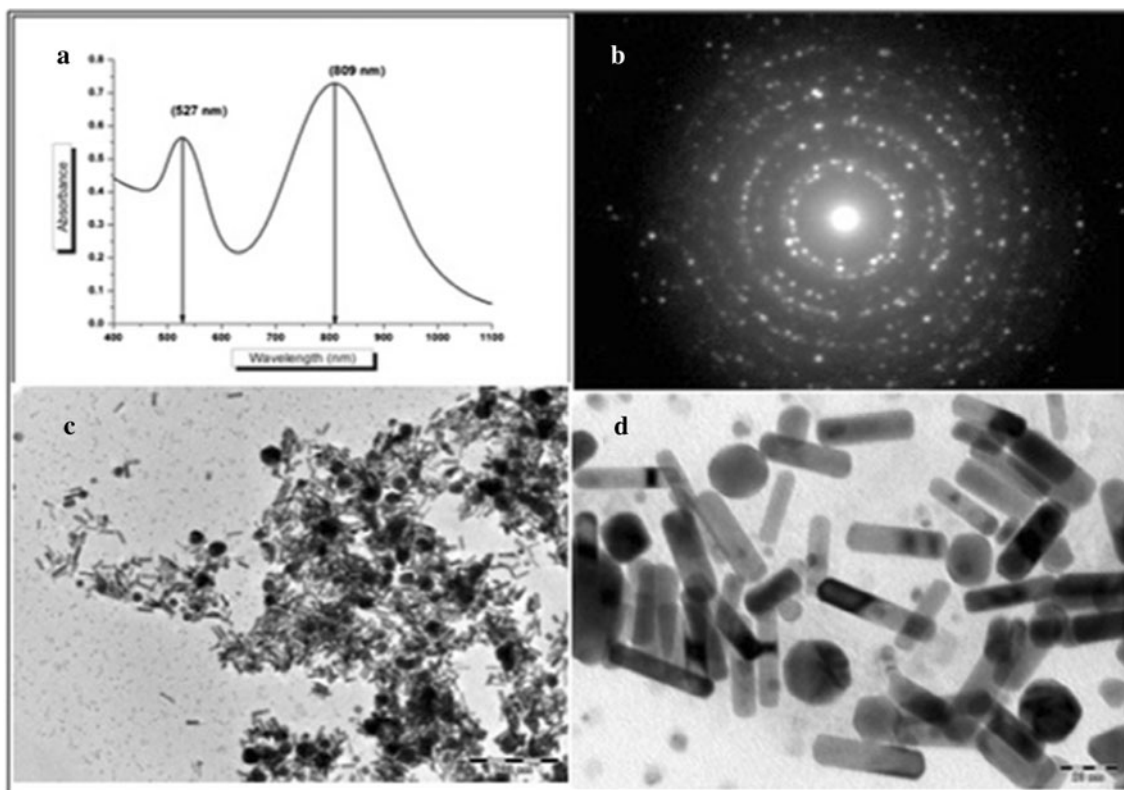


Fig. 1 a UV–Vis spectra of GNRs synthesized by seed mediated method with an aspect ratio of 4.01 [TSPR = 527 and LSPR = 809 nm]. b The selective area energy dispersion (SAED)

pattern showing that the GNRs are crystalline. c TEM image of synthesized GNRs. d Focused TEM image of GNRs with aspect ratio in range of 4–5

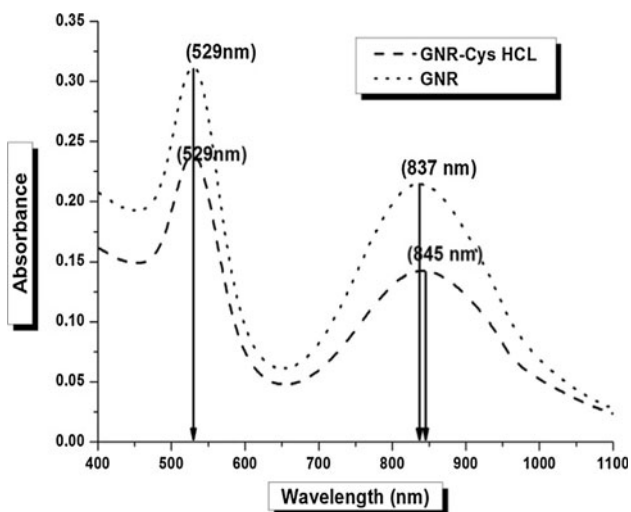
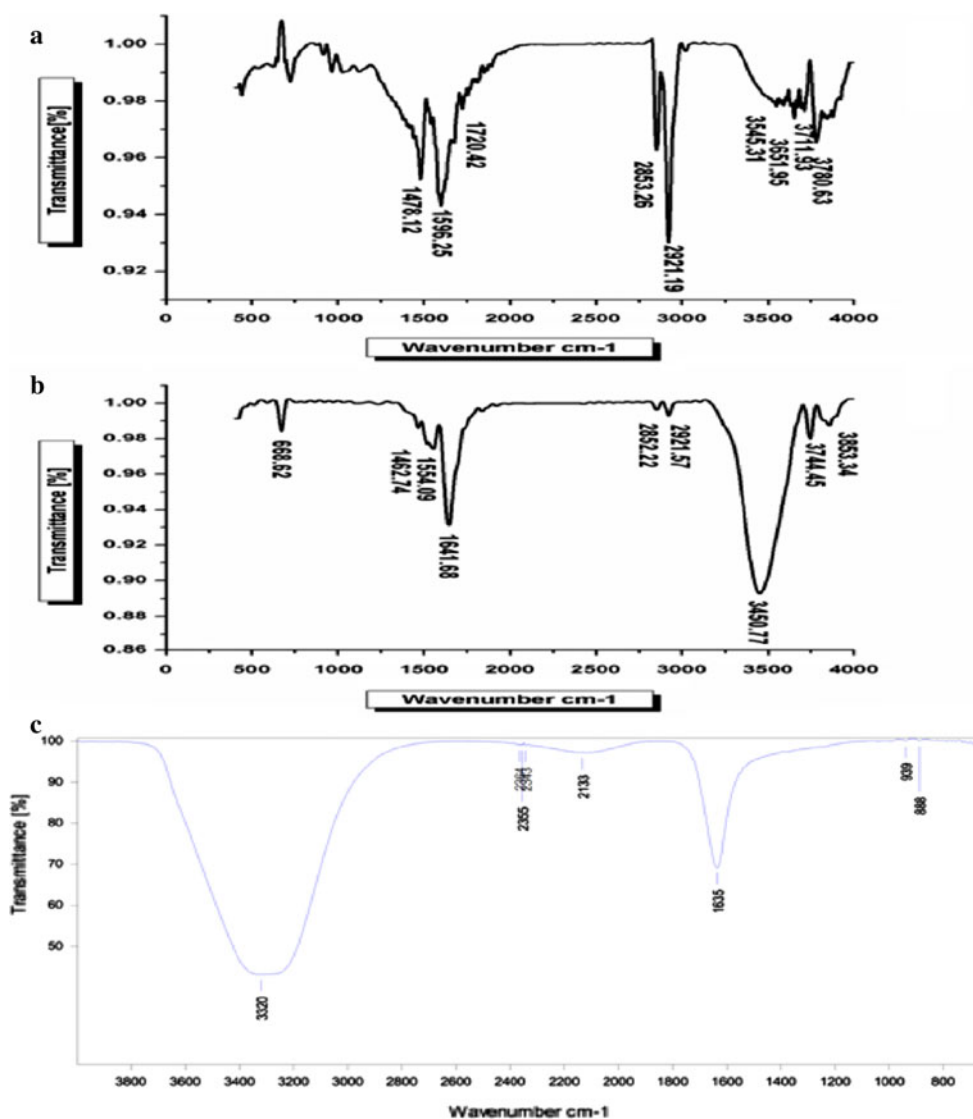


Fig. 2 UV-Vis spectra of GNRs and GNRs surface functionalized with Cys-HCl

Fig. 3 FTIR spectra of (a) GNR–cysteamine HCl conjugate (b) GNR(c) Cys-HCl



(Fig. 5a, b). Existence of weak bands at 1,653 and 1,713 cm^{-1} in activated folic acid (Fig. 5a) is a signature marker for asymmetric stretching vibrations of CH stretch and –NH stretch respectively. Appearance of strong peak at 1,595 and 1,720 cm^{-1} corresponds to asymmetric bending vibrations of –CO and stretching of 1° amines –NH visibly signify the fact that Folic acid must have adhered to GNR–Cys-HCl conjugate via an amide linkage. Nevertheless, an added significant fact is that folate has α and γ carboxylic acids and can be activated by DCC/NHS in the presence of DMSO. It’s a well known fact that γ carboxylic acids primarily get activated due to its higher reactivity [41]. Hence, we speculate conjugation of α carboxylic group of folic acid with amino group of cysteamine.

The schematic representation of the reaction between GNR–Cys-HCl and activated folated can be projected as displayed in Fig. 6.

3.4 Synthesis of GNR–FA–DOX complex

A relative study of the Fig. 7a, b exemplify the interaction of the GNR–Cys–FA–DOX complex is due to the manifestation of amide linkage. This may be due to appearance of the peak at $1,595\text{ cm}^{-1}$ which corresponds to the stretching of $=\text{CO}$ and $1,439\text{ cm}^{-1}$ corresponding to $=\text{CO}$ stretch of anhydride. The peak shift from $2,350\text{ cm}^{-1}$ (Fig. 6a) to $2,923\text{ cm}^{-1}$ (Fig. 6b) corresponds to the bending of $-\text{NH}_2$ (secondary amines) and $2,349\text{--}2,856\text{ cm}^{-1}$ corresponds to primary $-\text{NH}_2$. The most essential consideration is the formation of amide linkage ($-\text{CONH}$) due to interaction between $-\text{COOH}$ of doxorubicin and $-\text{NH}_2$ of surface

orchestrated GNRs. In Fig. 5b the emergence of peak at $1,595$ and $1,720\text{ cm}^{-1}$ symbolize asymmetric vibrations of $-\text{CONH}$ bends. This finding supports our speculation. Above findings can be schematically gauged as shown in Fig. 8.

3.5 Drug loading efficiency

Surface orchestrated GNRs with Cys-HCl and FA where loaded with DOX and centrifuged at $5,000\text{ rpm}$ and then purified further by dialysing it using 10 kDa membranes. After taking into account the mean values and carrying out

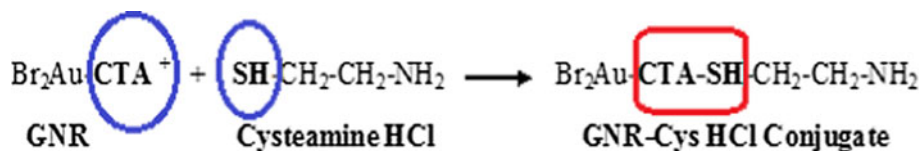


Fig. 4 Schematic representation of the reaction between GNR and cysteamine HCl. CTA^+ of GNR interacts with SH of cysteamine HCl to Form a CTA-SH bond i.e. thiol bond

Fig. 5 FTIR spectra of
(a) Activated FA
(b) GNR–Cys–FA complex

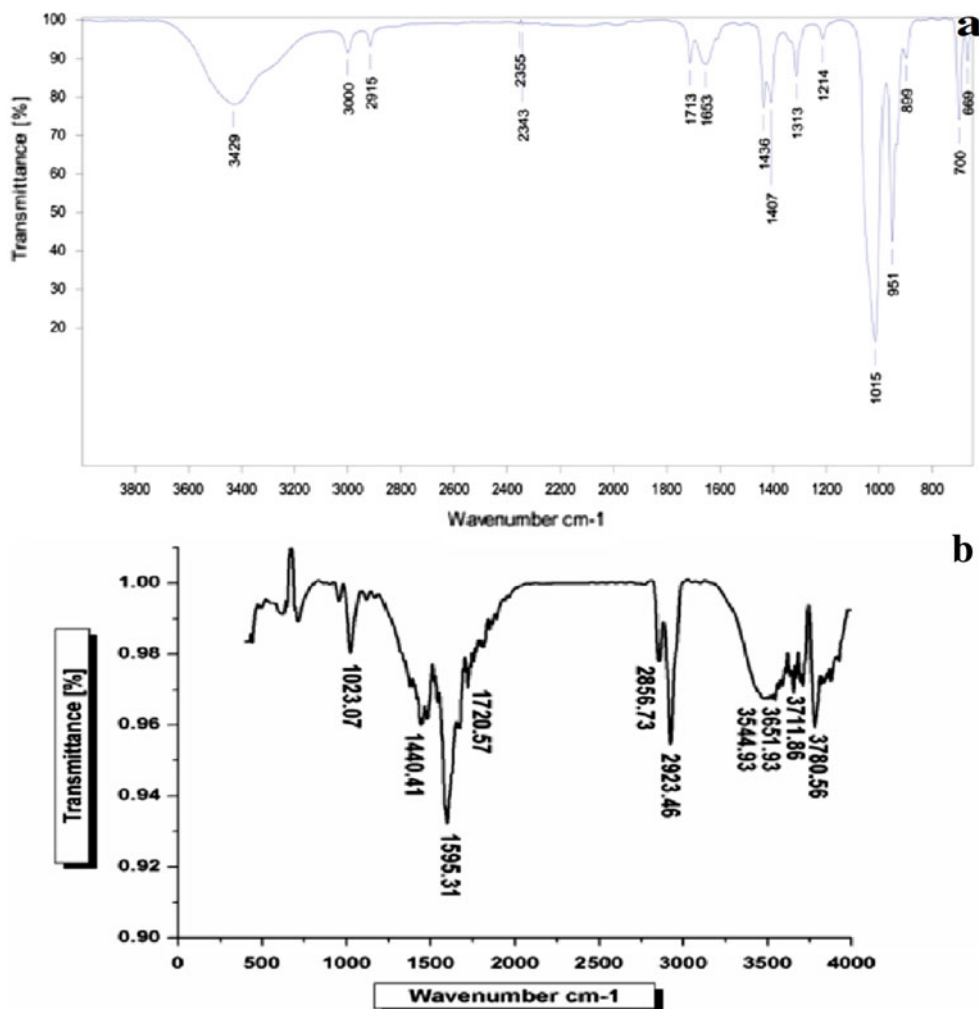


Fig. 6 Schematic diagram between GNR–Cys–HCl and Activated FA the free amino group of Cys–HCl interacts with α Carboxylic acid group of activated FA to form a CONH i.e. amide linkage

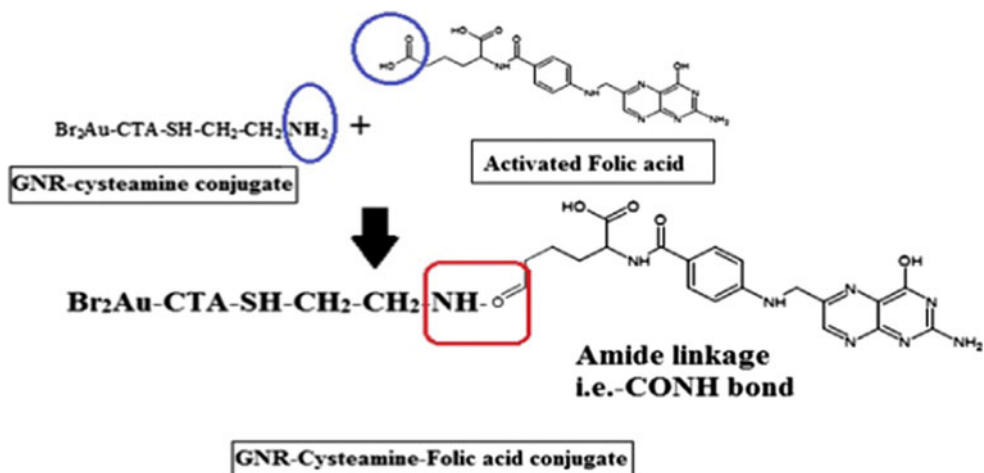


Fig. 7 FTIR Spectra (a) DOX (b) GNR–FA–DOX complex

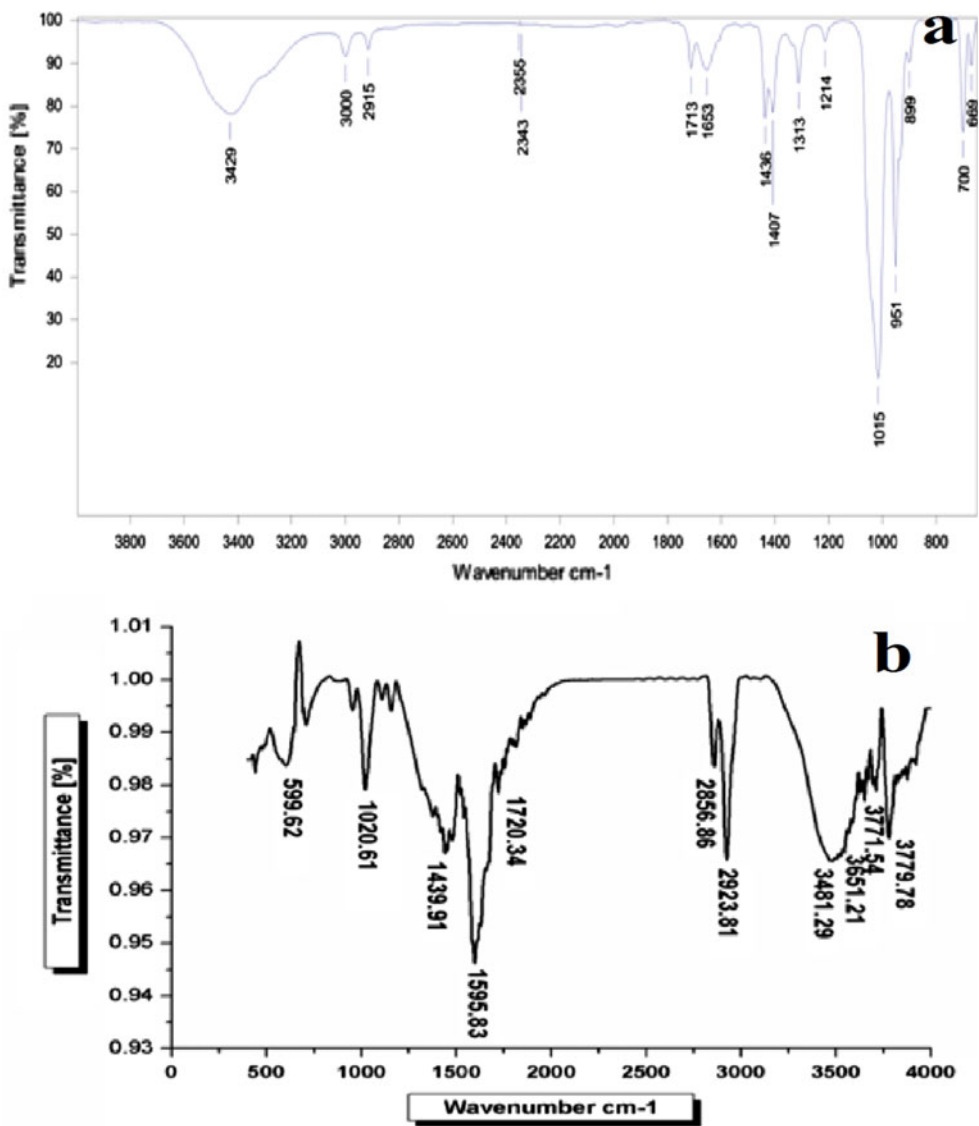


Fig. 8 Schematic illustration of interaction between GNR–Cys–A conjugate and DOX, the free amino end of FA reacts with carboxylic acid group in anaerobic environment to form an amide linkage which is pH sensitive

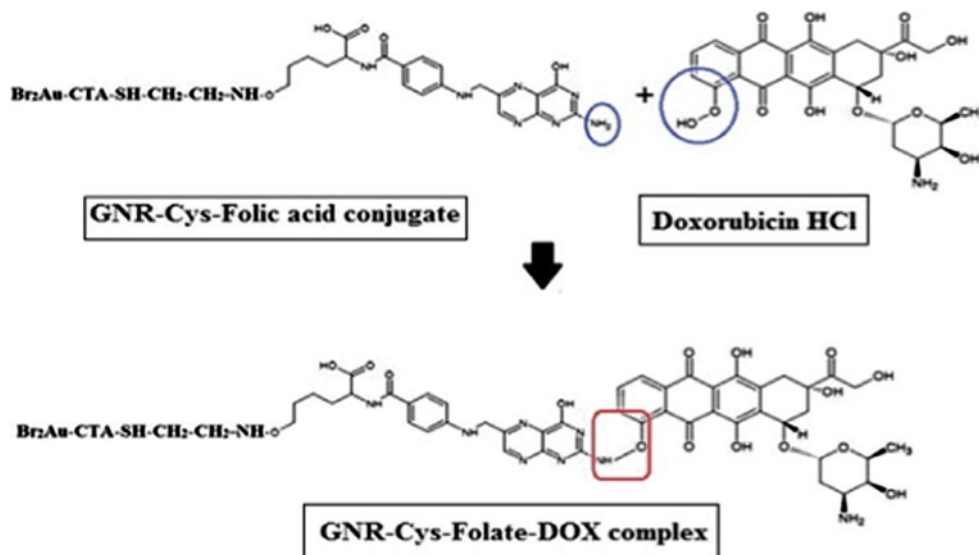
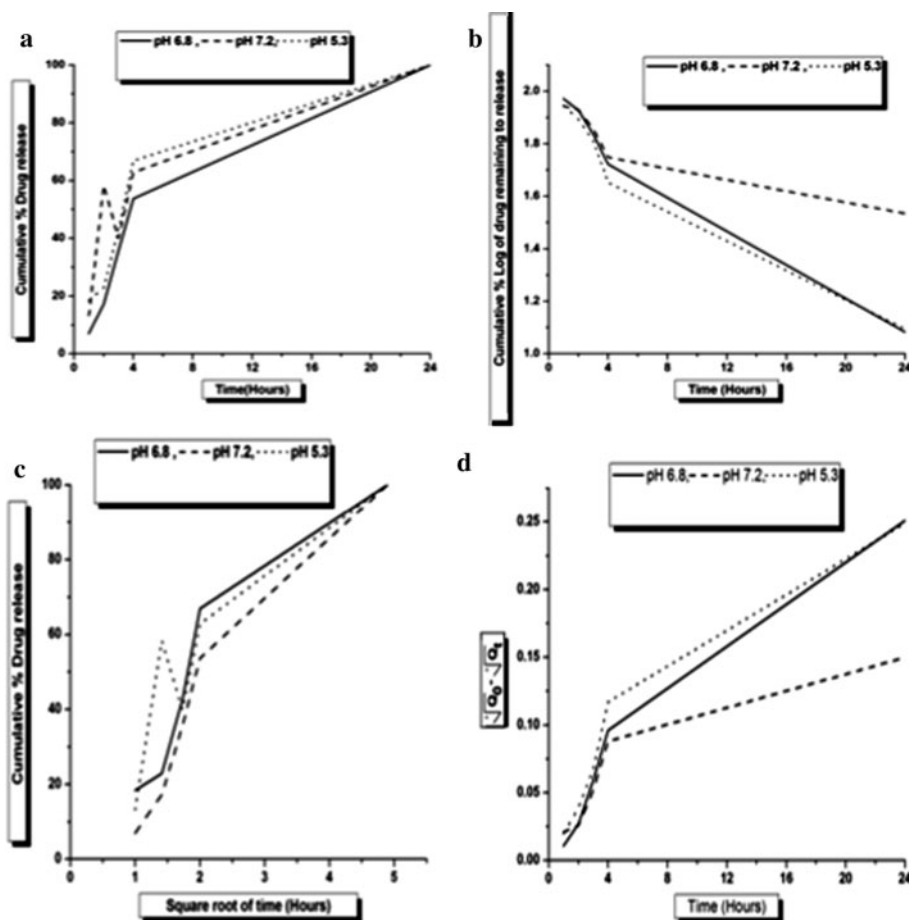


Fig. 9 Comparative drug release kinetics model of DOX released from GNR–Cys–FA–DOX Complex at pH 5.3, 6.8 and 7.2 (a) zero order (b) first order (c) Higuchi and (d) Hixson–Crowel model



significant statistical analysis. The calculated amount of drug loaded onto GNRs is 0.123 mM. Using Eq. (1) mentioned in “Materials and methods”; that drug loading efficiency was calculated to be 97.73 %.

3.6 Drug release kinetics

In vitro release profile at 37 °C of GNR–Cys–FA–DOX was studied using various statistical tools at pH 6.3, 6.8 and

7.2 respectively for duration of 24 h with an interval of 1 h. The kinetics of the drug release was decoded using Eqs. (2)–(5) which correspond to zero order, 1st order, Higuchi and Hixson–Crowel’s model respectively.

In order to scrutinise zero order drug release kinetics, the relation between time and cumulative percent of drug release was studied (Fig. 9a). It was speculated that the R² value at pH 6.8 was maximum followed by 7.2 and 5.3 as displayed in Table 1. Moreover, percent drug release at pH 6.8 followed a slow and gradual pattern of drug release with 52 % of drug released in 4 h and 99 % of drug was released after 24 h. The release studies at pH 7.2 exhibited comparatively faster and irregular rate of drug release with 59 % of drug release in 2 h which was followed by a drop in the rate of release at 3 h with 40 % and a rise is speculated in the 4th hour with 62 %. Moreover, pH 5.3 showed a dramatically high rate of drug release with a drug release percentage of 62 % in 4 h. On basis of these speculations we assume that the release kinetics is pH dependent [42] in case of zero order kinetics.

On studying the kinetics using the Eq. (3) for 1st order, a graph of time versus cumulative % log of drug remaining to be released was plotted. It was speculated that the R² value was consistent with the previous result i.e. at pH 6.8 (Table 1) followed by pH 5.3 and 7.2. Also, the relative

amount of drug remaining to be released was controlled in case of pH 6.8 and then in 5.3 as observed in Fig. 9b. The release pattern in 7.2 is comparatively faster. This suggested that the amide linkage between GNR–CYS–FA–DOX and GNR–CYS–FA is pH sensitive and fits the best in 1st order of kinetics. As, Cancerous cells exhibit a microenvironment which is acidic (pH 5.3–6.8) in nature when compared to that of inherent physiological pH i.e. 7.2 [6–11]. The bond formed between folate conjugated GNR and DOX is expected to be pH dependent. Hence, amount of DOX released in and around cancerous environment should be spectacularly high. Also, during folate-mediated endocytosis, the pH of the formed endosome is ~6.8. This adds to the specificity and thus increasing the therapeutic index of DOX.

Higuchi’s model is another statistical tool studied using Eqn. (4). A graph using square root of time versus cumulative % drug release is plotted (Fig. 9c). As observed in previous results, a similar high R² value at pH 6.8 is observed in this model with steady increase in drug release for 1st 4 h. Further speculations indicate that the release kinetics is faster as the time passes i.e. at 24 h (~4.8 h in Fig. 9c). Also, at pH 7.2 and 5.3 a drastic irregularity in the rate of drug release is noticed. The last tool used to study the release kinetics of DOX is Hixson–Crowel’s model using Eq. (5). Figure 9d explains clearly the amount of drug released at pH 6.8 is slow and steady with highest R² value as seen in Table 1. Additionally, pH 5.3 also shows gradual drug release rate with a lower R² value. On the other hand, pH 7.2 does not show a promising drug release profile (Fig. 9d).

Table 1 explains that the amount of drug released at pH 6.8 is high as it fits the best in the 1st order kinetics followed by pH 5.3. A relative study of Tables 1 and 2 reveals the fact that the release kinetics obeyed by DOX from GNR–Cys–FA Complex is 1st order kinetics at pH 6.8 which is the pH of endosomal environment has the maximum drug release rate with highest R² value followed by pH 5.3 which is the pH of perinuclear environment.

Table 1 A summary of R² values and percent drug release at pH 5.3, 6.8 and 7.2 in all the models

Models	pH value		
	pH 5.3	pH 6.8	pH 7.2
Zero order	0.771	0.8526	0.7035
First order	0.9539	0.9762	0.9261
Higuchi	0.8603	0.9261	0.779
Hixson–Crowel	0.9142	0.9475	0.8391

All the values are based on the Fig. 9. The values listed above are values of coefficient correlation (R²) obtained from release data from various mechanism of drug release

Table 2 A summary of percent drug release at pH 5.3, 6.8 and 7.2 in all the models

Time (h)	Models											
	Zero order (% drug release)			1st order (% drug remaining to release)			Higuchi (% drug release)			Hixson–Crowel $\sqrt[3]{Q_0} - \sqrt[3]{Q_t}$		
	5.3	6.8	7.2	5.3	6.8	7.2	5.3	6.8	7.2	5.3	6.8	7.2
1	20	8	10	1.92	1.98	1.92	22	18	12	0.02	0.03	0.03
2	40	20	59	1.87	1.88	1.85	62	70	60	0.03	0.05	0.04
3	58	30	40	1.75	1.78	1.74	70	80	76	0.04	0.07	0.05
4	62	52	62	1.67	1.68	1.65	84	92	83	0.05	0.10	0.08
24	78	99	98	1.12	1	1.3	92	99	95	0.23	0.25	0.16
R ²	0.77	0.85	0.70	0.95	0.97	0.92	0.86	0.92	0.77	0.91	0.94	0.83

All the values are based on the Fig. 6

pH dependent firing of drugs is a cardinal attribute ideal drug delivery machines particularly in cancer thermotherapy [22, 43]. DOX was found to be enhanced at pH 6.8. However, the extent of drug release (following 1st order) was faster at pH 6.8 than other two pH. After the injection of the GNR–FA–DOX conjugate, the first contact occurs with blood components at physiological pH (7.2). Here, DOX remains attached at the surface of GNRs for longer time, reducing the non-specific hostile effects of DOX. Upon entry into the cancer cells via endocytic pathway major amount of drug is released at pH 6.8. Most of the tumour environments were found to be acidic (pH 4.5–6.5 depending on the type of tumours).

4 Conclusions

DOX conjugated to FA orchestrated thiol-stabilized GNRs were synthesized and characterized using UV–Vis spectroscopy and FTIR. GNRs were successfully synthesized with an aspect ratio 4–5 and were surface functionalized using Cys–HCl. The attachment of Cys–HCl to GNR is via thiol bond as verified by FTIR. Whereas, amide linkage is involved in anchoring FA to GNR–Cys conjugate and DOX to GNR–Cys–FA conjugate which was confirmed using FTIR. These DOX conjugated GNR–Cys–FA exhibited remarkably higher pH dependent in vitro drug release kinetics at pH 6.8 in all the four statistical tools followed by pH 5.3 and 7.2. The most suitable environment for drug release was found to be pH 6.8 (endosomal environment) followed by pH 5.3 (perinuclear environment) and finally pH 7.2. A comparative computation of coefficient of correlation gave a clear idea that the release pattern of DOX followed the 1st order kinetics. These multifunctional DOX conjugated GNR–Cys–FA may also be used to improve imaging contrast or for synergistic photo-thermal cancer therapy.

Acknowledgments Authors wish to acknowledge the financial support provided by the authorities of SICES, Ambernath and specially Mr. K.M.S. Nair (President of SICES) and K.M.K Nair to carry out this project. We thank Dr. Lalla for carrying out TEM analysis for GNRs at RRCAT, Indore. A special thanks to SAIF IIT Bombay, for carrying out ICP-AES and FTIR analysis.

References

- Kataoka K, Kwon G, Yokoyama M, Okano T, Sakurai Y. Block copolymer micelles as vehicles for drug delivery. *J Control Release*. 1992;24:119–32.
- Kwon GS, Okano T. Polymeric micelle as new drug carriers. *Adv Drug Deliv Rev*. 1996;16:107–16.
- Yoo HS, Oh JE, Lee KH, Park TG. Biodegradable nanoparticles containing doxorubicin–PLGA conjugates for sustained release. *Pharm Res*. 1999;16:1114–8.
- Minko T, Kopeckova P, Pozharov V, Kopecek J. HPMAs copolymer bound adriamycin overcomes MDR1 gene encoded resistance in a human ovarian carcinoma cell line. *J Control Release*. 1998;54:223–33.
- Verdiere C, Dubernet C, Nemati F, Poupon MF, Puisieux F, Couvreur P. Uptake of doxorubicin from loaded nanoparticles in multidrug resistant leukemic murine cells. *Cancer Chemother Pharmacol*. 1994;33:504–8.
- Song C, Lyon JC, Luo Y. Intra and extracellular pH in solid tumors: influence on therapeutic response. In: Teicher BV, editor. *Drug resistance in oncology*. New York: Marcel Dekker; 1993. p. 25–51.
- Song CW, Park HJ, Ross BD. Intra and extracellular pH in solid tumors. In: Teicher BV, editor. *Antiangiogenic adnets in cancer therapy*. Totowa: Humana; 1998. p. 51–64.
- Webb SD, Sherratt JA, Fish RG. Mathematical modeling of tumour acidity: regulation of intracellular pH. *J Theor Biol*. 1999;196:237–50.
- Gilles RJ, Raghunand N, Karczmar GS. MRI of the tumor microenvironment. *J Magn Reson Imaging*. 1999;16:430–50.
- Svastove E, Hulikova A, Rafajova M. Hypoxia activates the capacity of tumor associated carbonic anhydrase IX to acidify extracellular pH. *FEBS Lett*. 2000;19:35–439.
- Aisenberg AC. *The glycolysis and respiration of tumors*. Nature. 1961;261:702–5. New York: Academic Press.
- Kim GE, Lyons JC, Levitt SH, Song CW. Effects of amiloride on intracellular pH and thermosensitivity. *Int J Radiat Oncol Biol Phys*. 1991;20:541–9.
- Gabizon, Horowitz AT, Goren D, Tzemach D, Man-delbaum-Shavit F, Qazen MM, Zalipsky S. Targeting folate receptor with folate linked to extremities of poly(ethyleneglycol)-grafted liposomes: in vitro studies. *Bioconjug Chem*. 1999;10:289–98.
- Guo W, Lee T, Sudimack JJ, Lee RJ. Receptor-specific delivery of liposomes via folate–PEG–chol. *J Liposome Res*. 2000;10:179–95.
- Lu Y, Low PS. Folate targeting of haptens to cancer cell surfaces mediates immunotherapy of syngeneic murine tumors. *Cancer Immunol Immunother*. 2002;51:153–62.
- Lee RJ, Low PS. Folate-mediated tumor cell targeting of liposome-entrapped doxorubicin in vitro. *Biochim Biophys Acta*. 1995;1233:134–44.
- Cummings J, McArdle CS. Studies on the in vivo disposition of adriamycin in human tumors which exhibit different responses to the drug. *Br J Cancer*. 1986;53:835–8.
- Pandey S, Oza G, Kesarkar R, Gupta A, Vishwanathan M, Shah R, Sharon M, Sharon M. Taguchi optimization method for tuning aspect ratios for synthesis of gold nano rods. *Arch Appl Sci Res*. 2012;4(2):965–70.
- Oza G, Pandey S, Shah R, Vishwanathan M, Kesarkar R, Sharon M, Sharon M. Tailoring aspect ratio of gold nano rods: impact of temperature, pH, silver ions, CTAB concentration and centrifugation. *Adv Appl Sci Res*. 2012;3(2):1027–38.
- Dubin CH. Special delivery: pharmaceutical companies aim to target their drugs with nano precision. *Mech Eng Nanotechnol*. 2004;126:10–2.
- Dass CR, Su T. Particle-mediated intravascular delivery of oligonucleotides to tumors: associated biology and lessons from gene therapy. *Drug Deliv*. 2001;8:191–213.
- Pandey S, Oza G, Mewada A, Shah R, Thakur M, Sharon M. Folic acid mediated synaphic delivery of doxorubicin using biogenic gold nanoparticles anchored to biological linkers. *J Mater Chem B*. 2013;1:1361–70.
- Courrier HM, Butz N, Vandamme TF. Pulmonary drug delivery systems: recent developments and prospects. *Crit Rev Ther Drug Carrier Syst*. 2002;19:425–98.
- Senior K. Nano-dumpling with drug delivery potential. *Mol Med Today*. 1998;4:321.

25. DA LV, Lynn DM, Langer R. Moving smaller in drug discovery and delivery. *Nat Rev Drug Discov.* 2002;1:77–84.
26. DA LV, McGuire T, Langer R. Small-scale systems for in vivo drug delivery. *Nat Biotechnol.* 2003;21:1184–91.
27. Xiao Y, Hong H, Matson VZ, Javadi A, Xu W, Yang Y, Zhang Y, Engle JW, Nickles RJ, Cai W, Steeber DA, Gong S. GNRs conjugated with doxorubicin and cRGD for combined anti-cancer drug delivery and PET imaging. *Theranostics.* 2012;8:757–68.
28. Ravi KMN. Nano and microparticles as controlled drug delivery devices. *J Pharm Sci.* 2000;3:234–58.
29. Costa P, Sousa LJM. Modeling and comparison of dissolution profiles. *Eur J Pharm Sci.* 2001;13:123–33.
30. Siepman J, Gopferich A. Mathematical modeling of bioerodible, polymeric drug delivery systems. *Adv Drug Deliv Rev.* 2001;48:229–47.
31. Dash S, Murthy PN, Nath L, Chowdhury P. Kinetic modeling on drug release from controlled drug delivery systems. *Acta Pol Pharm.* 2010;67(3):217–23.
32. Gallagher KM, Corrigan OI. Mechanistic aspects of the release of levamisole hydrochloride from biodegradable polymers. *J Control Release.* 2000;69:261–72.
33. Barua, et al. Particle shape enhances specificity of antibody-displaying nanoparticles. *Proc Natl Acad Sci USA.* 2013;. doi: [10.1073/pnas.1216893111](https://doi.org/10.1073/pnas.1216893111).
34. Daniel MC, Astruc D. Gold nanoparticles: assembly, supramolecular chemistry, quantum-size-related properties, and applications toward biology catalysis, and nanotechnology. *Chem Rev.* 2004;104:293–346.
35. Sharma V, Park K, Srinivasarao M. Colloidal dispersion of GNRs: historical background, optical properties, seed-mediated synthesis, shape separation and self-assembly. *Mater Sci Eng R.* 2009;65:1–38.
36. Link S, El-Sayed M. A size, temperature dependence of the plasmon absorption of colloidal gold nanoparticles. *J Phys Chem B.* 1999;103:4212–7.
37. Gans R. On the shape of ultramicroscopic gold particles. *Annalen Der Physik.* 1912;37:881–900.
38. Templeton AC, Hostelter MJ, Kraft CT, Murray RW. Reactivity of monolayer-protected gold cluster molecules: steric effects. *J Am Chem Soc.* 1998;120:1906–11.
39. Johnson SR, Evans SD, Mahon SW, Ulman A. Alkanethiol molecules containing an aromatic moiety self-assembled onto gold clusters. *Langmuir.* 1997;13:51–7.
40. Colin BD, Evall J, Whitesides GM. Formation of monolayers by the coadsorption of thiols on gold: variation in the head group, tail group, and solvent. *J Am Chem Soc.* 1989;111:7155–64.
41. Bhattacharya R, Patra CR, Earl A, Wang S, Katarya A, Lu L, Kizhakkedathu JN, Yaszemski MJ, Greipp PR, Mukhopadhy D, Mukherjee P. Attaching folic acid on gold nanoparticles using noncovalent interaction via different polyethylene glycol backbones and targeting of cancer cells. *Nanomedicine.* 2007;3:224–38.
42. Aryal S, Grailer JJ, Pilla S, Steeber DA, Gong. Doxorubicin conjugated gold nanoparticles as water-soluble and pH-responsive anticancer drug nanocarriers. *J Mater Chem.* 2009;19:7879–84.
43. Ulbrich K, Subr V. Polymeric anti cancer drugs with pH controlled activation. *Adv Drug Deliv Rev.* 2004;56:1023–50.